Evidence of Three-Dimensional Asymmetries Seeded by High-Density Carbon-Ablator Nonuniformity in Experiments at the National Ignition Facility

D. T. Casey et al.

Phys. Rev. Lett. **126**, 025002 — Published 12 January 2021

DOI: 10.1103/PhysRevLett.126.025002

Evidence of Three-dimensional Asymmetries Seeded by HDC-ablator Non-uniformity in Experiments at the National Ignition Facility

D. T. Casey, [1] B. J. MacGowan, [1] J. D. Sater, [1] A. B. Zylstra, [1] O. L. Landen, [1] J. Milovich,[1] O. A. Hurricane,[1] A. L. Kritcher, [1] M. Hohenberger,[1] K. Baker, [1] S. Le Pape, [1] T. Döppner,[1] C. Weber,[1] H. Huang, [2] C. Kong,[2] J. Biener, [1] C. V. Young,[1] S. Haan,[1] R. C. Nora,[1] S. Ross,[1] H. Robey,[1] M. Stadermann,[1] A. Nikroo,[1] D. A. Callahan,[1] R. M. Bionta,[1] K. D. Hahn,[1] A. S. Moore,[1] D. Schlossberg,[1] M. Bruhn,[1] K. Sequoia,[2] N. Rice,[2] M. Farrell,[2] C. Wild[3]

1) Lawrence Livermore National Laboratory, USA
2) General Atomics
3) Diamond Materials

Inertial confinement fusion implosions must achieve high inflight shell velocity, sufficient energy coupling between the hotspot and imploding shell, and high areal-density ($\rho R = \int \rho dr$) at stagnation. Asymmetries in ρR degrade the coupling of shell kinetic energy to the hotspot and reduce the confinement of that energy. We present the first evidence that non-uniformity in the ablator shell thickness (~0.5% of the total thickness) in high-density carbon experiments is a significant cause for observed 3D ρR asymmetries at the National Ignition Facility (NIF). These shell thickness non-uniformities have significantly impacted some recent experiments leading to ρR asymmetries on the order of ~25% of the average ρR and hotspot velocities of ~100 km/s. This work reveals the origin of a significant implosion performance degradation in ignition experiments and places stringent new requirements on capsule thickness metrology and symmetry.

In inertial confinement fusion (ICF) experiments performed at the National Ignition Facility (NIF) [1], capsules of deuterium and tritium (DT) fuel are imploded to high densities and temperatures to initiate alpha-particle self-heating and fusion burn [2,3]. The indirect drive ICF concept uses a laser to irradiate a high-Z cylindrical hohlraum, which attempts to produce a nearly uniform, quasi-thermal, x-ray drive. The x-ray drive then ablates the outer layers of the capsule, compressing the remaining ablator and an inner layer of cryogenically frozen DT radially inward. This imploding shell converges on and compresses a gaseous DT region to form a hotspot. To achieve ignition, the DT hotspot must have high enough energy-density confined for adequate time to spark hotspot self-heating and start a burn wave through the dense DT shell. This requirement can be equivalently expressed as a condition of $P\tau$; where P is the hotspot pressure, a measure of the energy density, and τ is the confinement time of that energy [4,5]. To produce high $P\tau$, an implosion must have high inflight implosion velocity (v_{imp}), sufficient coupling between the inflight shell and hotspot, and high areal-density (or ρR defined as $\rho R = \int \rho dr$) at stagnation.

The coupling of the shell kinetic energy and the confinement of that energy are both degraded by three-dimensional (3D) ρR asymmetry. Recent analysis using a simplified two-piston system shows [6] that in the limit of weak-alpha heating: $\frac{P\tau}{P\tau_{1D}} \approx (1-f^2)$ and $\frac{Y}{Y_{1D}} \approx (1-f^2)^{10/3}$, where $\frac{Y}{Y_{1D}}$ is the yield (Y) normalized by idealized 1D symmetric yield (Y_{1D}) and $f = \frac{\rho R_{max} - \rho R_{min}}{\rho R_{max} + \rho R_{min}} \approx \frac{v_{HS}}{v_{imp}}$. Here ρR_{max} and ρR_{min} are the maximum and minimum areal-densities of the dense shell, respectively; v_{HS} is the bulk velocity of the burning hotspot near peak convergence, and v_{imp} is the peak implosion velocity. These relationships reveal that a ~ 25% asymmetry in $\delta\rho R/\rho R$ (or an observed hotspot velocity v_{HS}~100 km/s for an implosion velocity of v_{imp}~400 km/s) can result in a ~7% loss in hotspot internal energy corresponding to a ~22% reduction in no-alpha yield. Furthermore, the impact of this degradation can be much larger if alpha heating is significant. For example, this level of asymmetry is predicted to result in a ~38% reduction in total yield, including estimates for alpha heating [7], for an implosion with an unperturbed neutron yield of 2e16 and neutron down-scattered ratio [8-10] (or DSR, which is related to the $\rho R[g/cm^2]$~ 0.2 DSR[%]) of DSR=3.3%, resulting in a yield of about 1.3e16. Experiments with intentional asymmetries [11,12] have shown yield degradations consistent with these arguments. Furthermore, trends over all experiments suggest low-mode asymmetries are among several important degradations in current experiments ICF at the NIF, as also recently shown with Compton radiography measurements [13].

Percent level deviations from perfect radiation-drive or target uniformity can seed asymmetries and cause them to grow during the implosion. This in turn reduces the hotspot/shell coupling and degrades confinement of that energy resulting in reduced overall performance. In fact, experiments often exhibit signatures of asymmetry and understanding their origin is of paramount importance in mitigating and removing their impact. Herein, we show new evidence that ablator shell-thickness non-uniformity is an important cause of observed lowmode asymmetries. When combined with other recent results [14] that identified the principal causes of radiation drive non-uniformity, this newly identified ablator thickness seed appears among the primary causes of 3D asymmetries.

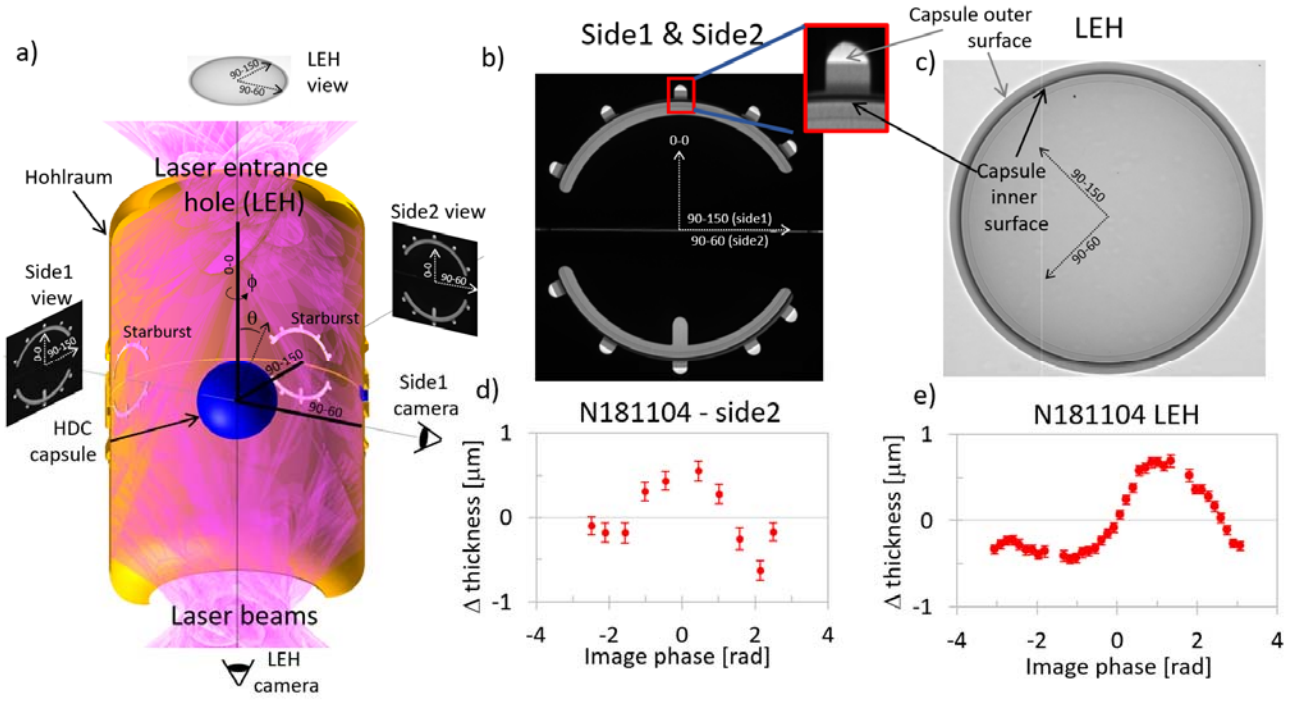

Figure 1: a) Schematic of hohlraum, capsule, and radiograph lines-of-sight. b-c) Radiograph measurements of the HDC capsule used on shot N181104 from the side and LEH views. d-e) HDC capsule thickness asymmetries measured from the radiographs in b-c.

The experiments described herein used 192 NIF laser beams to indirectly drive a 6.20-6.72 mm diameter depleted uranium (DU) hohlraums, each with a thin Au-coating. The laser beams enter through laser entrance holes (LEH) at each end of the cylindrical hohlraum that ranged from 3.64 - 4 mm in diameter depending on the specific design details of each platform. In each experiment, the hohlraum was filled with helium gas between 0.3-0.45 mg/cc fill to tamp the hohlraum wall. Inside the hohlraum is a 55-65 μm thick cryogenically frozen deuterium-tritium ice layer of density 0.255 g/cm^3 inside a 1000-1100 μm inner radius high-density carbon (HDC)[15],[16-27] capsule. The capsules used were between 76-80 μm thick predominantly made of 3.45 g/cm^3 micro- or 3.33 g/cm^3 nano-crystalline grains. The shells included a layer doped with W to ~0.3-0.4% atom-percent in a ~20 μm thick layer to shield the DT-ablator interface from hard x-rays to maintain a favorable Atwood-number reducing high-mode DT-ablator instability growth [28].

Efficient conversion of inflight kinetic energy into hotspot internal energy requires keeping drive asymmetry limited to sub-percent levels during the implosion. Recently, a study [14] revealed the role of x-ray drive radiation asymmetries resulting from peak laser power balance and diagnostic window losses as a principle cause of observed asymmetries [14][29]. Similar work in direct-drive implosions at OMEGA have tied observed low-mode asymmetries to inducements by the drive from laser beam pointing and power/timing fluctuations [30,31]. Specifically with regard to the experiments at the NIF [14], roughly ~75% of select cases were explained by radiation non-uniformities, while ~25% appear to be dominated by some other unidentified mechanisms. Further, several recent experiments seemed less likely to be explained by radiation asymmetries alone motivating a search for other causes including the possibility of capsule inducements as described below.

To measure the HDC shell thickness uniformity, several methods are employed. One places the capsule on a radiographic film plate and uses backlit x-ray radiography (contact radiograph) [32,33]. This technique can also measure the concentricity of the inner and outer surfaces to about ~0.15 μm and can only view the capsule from a single view at present making it useful for detecting problem capsules and for performing overall batch surveillance. After the target is built and is undergoing preparations to be shot, the phase contrast enhanced x-ray radiography [34-36] technique is used to characterize the shell thickness in 3D in the "cryo-tarpos" layering and imaging station from three orthogonal views [36]. The HDC shell is viewed through the LEH along the hohlraum axis and through "starburst" cutouts at the hohlraum equator, or "side views," as illustrated by Figure 1a. Figure 1b shows an x-ray radiograph from capsule KC461-03 that was used on experiment N181104 viewed from one of the side views, while Figure 1c shows a radiograph along the LEH view. Figure 1d and e show the HDC shell Δ thickness (value minus the average) as a function of angle along the image (where phase=0 is the right hand axis of the image and the angle increases counter clock-wise from there). Fitting the available data results in an amplitude of 0.78 ± 0.2 % out of an average thickness of 78 μm [37].

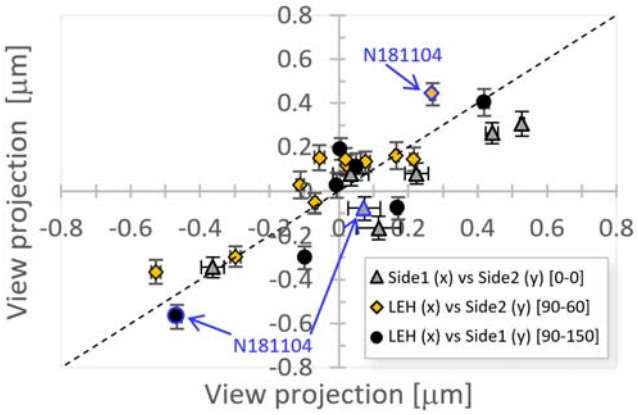

Figure 2: A comparison between the 90-150 component of the capsule thickness mode-1 determined from the fit projections along the common 90-150 axis of the orthogonal LEH and side1 radiographs (black circles), the 90-60 component from the LEH and side2 radiographs along their common axis (orange diamonds), and the 0-0 component from the side1 and side2 data along their common axis (grey triangles).

To build more confidence in the capsule thickness asymmetry measurements, the three orthogonal views from the cryo-tarpos layering station were fitted with a pure mode-1 and compared along their common axes for the capsules used in this dataset. Figure 2 shows the 90-150 component of the thickness mode-1 (where 90 is the polar angle in degrees, and 150 is the azimuthal angle) from the LEH view compared to the side1 view, the 90-60 component determined from the LEH and side2 views, and the 0-0 component determined from the side1 and side2 views. The scatter in the data points is larger than the statistical uncertainty because of errors in the edge-finding routine used to identify the inner and outer surfaces and background issues not captured by statistical uncertainty of the data. The root-mean square (RMS) of all available HDC data when comparing the two side views to LEH views is ~0.15 µm. Figure 2 also compares the side views to each other along the 0-0 direction and the RMS is ~0.3 µm. Because these values are larger than the statistical uncertainty, we take these comparisons to be representative of the total error in determining the mode-1 asymmetry of the capsule thickness including non-statistical fluctuations from effects described earlier. Further, the LEH data is more extensive and of generally higher quality and so we infer the LEH view error is 0.1 µm and the side view error is 0.15 µm.

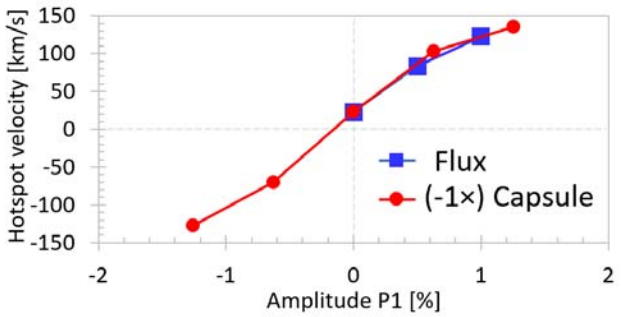

Figure 3: Simulations of HDC capsule thickness induced hotspot velocity versus the amplitude of the shell thickness asymmetry (red circles) with an intentional sign change for easier comparison to the capsule radiation flux induced hotspot velocity versus angle (blue squares). The simulations show that HDC thickness will drive a hotspot velocity very similarly to the previously identified capsule flux asymmetries.[14,38]

Two-dimensional simulations using the radiation hydrodynamics code HYDRA [39] can calculate the predicted impact of capsule thickness and hence ρR asymmetries on implosions like those observed here. Figure 3 shows the simulated hotspot velocity as a function of the capsule mode-1 amplitude (red circles) compared with simulations for an 1100 µm inner radius HDC capsule. For this particular HDC platform, the predicted sensitivity is ~110 km/s/%-m1 (kilometer per second per percent mode-1) becoming non-linear at high initial seed amplitude [40][41]. Figure 3 also shows the hotspot velocity sensitivity as a function of applied mode-1 flux asymmetries (opposite sign) in units of % relative to the peak flux and applied over the entire pulse. The results are consistent with prior simulation studies of radiation flux induced asymmetries [38].

Interestingly, the sensitivity to flux and capsule thickness is about the same but with opposite phase. This phase difference is because the initially thicker capsule side implodes to a slower peak velocity than the thinner side resulting in a delay in reaching peak convergence. This is shown by examining a 1st order solution [42] (neglecting the effect of late time ablation pressure or "coast") to the spherical rocket equations: $v_{imp} \sim 2\pi R_0^2 p_{max} t_{off}/M_0$, where R_0 is the initial capsule radius, p_{max} is the peak ablation pressure, t_{off} is the time of peak ablation pressure, and M_0 is the initial capsule and DT payload mass. When perturbed for small changes in the initial mass (dm_0/m_0), the change in v_{imp} becomes $dv_{imp}/v_{imp} \sim -dm_0/m_0$. Therefore, somewhat counterintuitively, the initially thicker side will reach lower ρR because of spherical convergence as its implosion trajectory is delayed by the initially weaker acceleration. Then as hotspot pressure builds the lower ρR part of the shell is decelerated more than the higher ρR part, further amplifying the difference. The result is that by peak neutron production the resultant hotspot velocity becomes directed toward the lower ρR or the initially thicker side. This is

the opposite direction of a flux (F) asymmetry (dF/F), which will typically drive the side of the capsule faster where the flux is higher like $dv_{imp}/v_{imp} \sim \frac{7}{8} dF/F$, where the 7/8 comes from the relative sensitivity of flux and ablation pressure [43]. This predicts a net hotspot velocity directed away from the initially higher flux side. Note that numerical calculations are somewhat less sensitive (~30%) than these rough estimates but that the sensitivity and sign difference between flux and capsule mass asymmetry is preserved. Furthermore, simulations with HYDRA show that the presence of graded dopant can further reduce the sensitivity of outer surface perturbations because the ablation rate stays higher longer as it must traverse more undoped material before reaching the doped layer on the initially thicker side where the ablation rate will drop. This ablation rate effect with doped layers helps explain why the sensitivities of flux perturbations and mass perturbations, as calculated, are nearly equal and opposite phase in Figure 3.

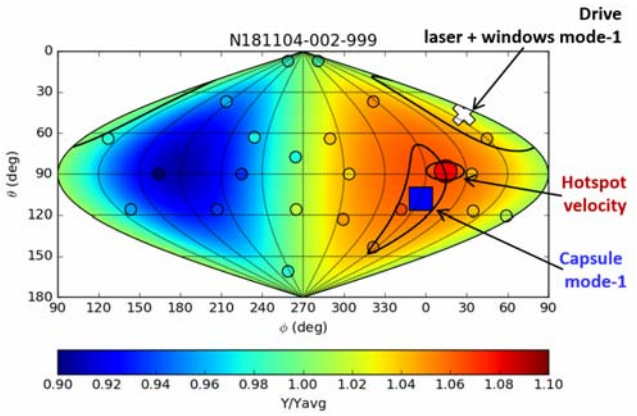

Figure 4: RTNAD activation data for shot N181104 showing a significant asymmetry aligned principally toward ~90-0. Also shown is the hotspot velocity (circle) that aligns with the RTNAD data. The drive + windows asymmetry (plus indicates direction of less intense drive) and capsule (square indicates direction of thicker side) mode-1 asymmetries are also shown. The capsule asymmetry most closely aligns with the observed implosion asymmetry in this experiment.

Experiments often show evidence of significant ρR asymmetry and resultant hotspot velocity. Shot N181104 presents an interesting example as is not easily explained by drive and diagnostic window asymmetries and so is among the anomalous ~25% of cases [14]. Observations of the ρR asymmetry are made using the anisotropy of the emitted 14 MeV yield with the real time neutron activation detector suite (RTNADs), a more precise and larger activation detector suite to its predecessor FNADs [44]. The observed RTNAD data for N181104 is presented in Figure 4 along with a $\ell \leq 2$ Y_{lm}-mode fit presented in NIF angular coordinates, theta and phi. The RTNAD data measures the unscattered neutron yield, which is sensitive to path integrated areal-density (ρL) via neutron attenuation, where: $Y/Y_{avg} \approx 1 - 0.2 \times \delta\rho L[g/cm^2]$. However, the exact relationship to δρR requires a model of the source and scattering material geometry. Nevertheless, the data clearly indicate significant variations in Y/Y_{avg} and therefore shell ρR anisotropies (blue areas are high ρR, and red low ρR). The data show a large ρR asymmetry aligned along the equator (θ~90°) with a high ρR region near ϕ~180° and a low ρR around ϕ~0°. The hotspot velocity is determined using neutron time-of-flight (nTOF) measurements of the Doppler shifted DT neutron spectrum [10] and is also indicated on Figure 4 and closely aligns with the low-ρR region consistent with the observations of Rinderknecht [45]. The direction of the radiation drive asymmetry including the impact of diagnostic windows and delivered laser energy balance calculated using a 3D view factor model [14] is also indicated Figure 4. The drive asymmetry cannot fully explain the direction and magnitude of the observed asymmetry for N181104. However, the direction of the observed pre-shot HDC shell asymmetry mode-1, described in Figure 1d-e, aligns closely with the direction of the ρR asymmetries observed at peak compression as indicted in Figure 4 strongly suggesting a linkage.

To determine if the magnitude of the HDC shell asymmetry correlates with the observed hotspot velocity with a larger data set of recent experiments, the known radiation drive asymmetry [14] from peak laser power fluctuations and diagnostic window losses is estimated and then removed from the hotspot velocity vector [46] assuming that the relationship to the seeds remain linear [47]. The magnitude of that residual, or unexplained, hotspot velocity is compared to the magnitude of the HDC shell asymmetry [48] in Figure 5. The residual hotspot velocity of N181104 is 92 km/s and with an amplitude of 0.78%, consistent with the overall observed trend in the broader dataset. This dataset also shows that the total hotspot velocity is correlated with the apparent ρR asymmetry determined from the RTNAD instrument suite, similar to earlier datasets [45]. Additionally, the RTNAD inferred asymmetry and asymmetry in the observed DSR measurements with the neutron spectrometer suite [8,10] are also correlated. The inferred ion temperature width from the Doppler broadened DT neutron spectrum suggests higher order flows induced by mode-1 asymmetries [12,49] and work is ongoing to compare these measurements to the hotspot velocity including a newly installed nTOF line-of-sight. Notably, this dataset shows considerable hotspot velocity sensitivity to the capsule mode-1 asymmetry 140 ± 30 km/s/% and a large fraction of the experiments in this particular dataset seem to be impacted by this important new seed. The sensitivity determined from the data in Figure 5 is consistent with the simulations in Figure 3 when considering the spread in the data. The spread in the data is due to known sensitivities [6] of the hotspot velocity to platform parameters like v_{imp} and DSR that are varying in this dataset, measurement uncertainties, and the non-linearity of the hotspot velocity to high initial seeds [38]. It is thought that the introduction and growth of low mode HDC thickness asymmetries occur either in the coating or polishing phases of capsule manufacture. The high empirically determined sensitivity motivates significant efforts to understand and mitigate.

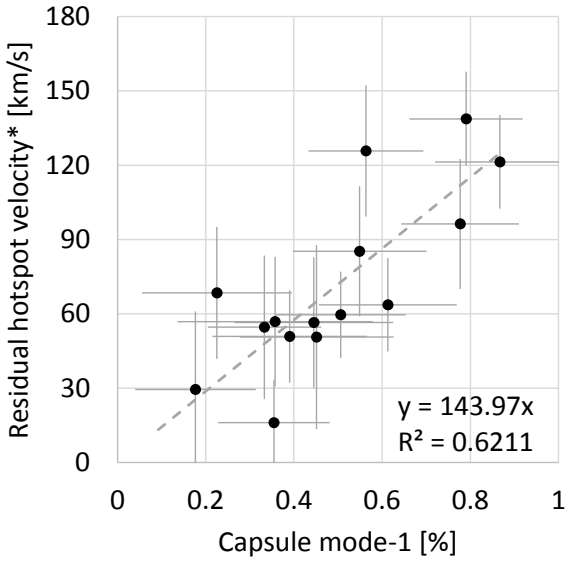

Figure 5: Residual hotspot velocity (defined as the measured velocity vector with known seeds from radiation drive asymmetries [14] subtracted) for recent HDC experiments from HyB[27,50], [51], HyE[52], and I-raum campaigns [24].

It should be emphasized that the potential impact of a shell induced asymmetry on the performance of an implosion is a strong function of the importance of alpha particle self-heating and the proximity to ignition. As noted earlier, a ~100 km/s hotspot velocity is expected to have a significant reduction (~38%) in total yield for an implosion that would have produced about ~2e16 and 3% DSR, otherwise. However, a similar analysis predicts that impact would be catastrophic for an implosion that might otherwise produce 2e17 total yield, instead suffering a ~10× reduction from a similar initial perturbation. In other words, perturbations on the order of those observed in Figure 5 could reduce a potential ~MJ class implosion to ~100 kJ of fusion yield. Therefore, this work places stringent new requirements on the capsule thickness symmetry that must become even more restrictive if implosion performances are to be improved significantly beyond the best implosions to date. Furthermore, improvements in metrology to measure thickness uniformity may be needed. To that end, the development of optical and infrared interferometry techniques is underway and early results are encouraging.

In summary, ablator shell thickness non-uniformities, have been revealed as a significant cause for 3D asymmetries in HDC ablator implosion experiments at the NIF. This finding, while specific to HDC experiments, is likely applicable to all ablator (HDC, CH, Be, etc.) designs. However, the potential impact may vary due to ability to manufacture sufficiently symmetric shells relative to the total shell thickness and the capability to metrologize as-built shells to required accuracy. Additionally, this newly identified seed has significantly perturbed recent implosions. To mitigate this issue, ongoing improvements in metrology will help identify problematic capsules earlier in the target fabrication process so that they can be excluded, and work is currently underway to determine and alleviate the root cause. Along with the sources of radiation drive asymmetries that have also recently been identified [14], we can now explain a significant majority of the hotspot velocities and ρR asymmetries observed in HDC ICF experiments at the NIF and are working to mitigate their sources.

The authors sincerely thank the NIF operations staff who supported this work. This work was performed under the auspices of the U.S. Department of Energy by Lawrence Livermore National Laboratory under Contract DE-AC52-07NA27344 and General Atomics under Contract DE-NA0001808.

References

[1] E. I. Moses, Journal of Physics: Conference Series **112**, 012003 (2008).
[2] J. D. Lindl, P. Amendt, R. L. Berger, S. G. Glendinning, S. H. Glenzer, S. W. Haan, R. L. Kauffman, O. L. Landen, and L. J. Suter, Physics of Plasmas **11**, 339 (2004).
[3] S. Atzeni and J. Meyer-ter-Vehn, *The physics of inertial fusion* (Oxford University Press, Oxford, 2004), International series of monographs on physics.
[4] J. P. Freidberg, *Plasma physics and fusion energy* (Cambridge University Press, Cambridge, 2007).
[5] R. Betti *et al.*, Physics of Plasmas **17**, 058102 (2010).
[6] O. A. Hurricane *et al.*, Physics of Plasmas **27**, 062704 (2020).
[7] B. K. Spears *et al.*, Physics of Plasmas **19**, 056316 (2012).
[8] M. G. Johnson *et al.*, Review of Scientific Instruments **83**, 10D308 (2012).
[9] J. A. Frenje *et al.*, Physics of Plasmas **17**, 056311 (2010).
[10] R. Hatarik *et al.*, Journal of Applied Physics **118**, 184502 (2015).
[11] D. Eder *et al.*, Journal of Physics: Conference Series **717**, 012014 (2016).
[12] Schlossberg and e. al, Submitted to Phys. Rev. Lett.
[13] R. Tommasini *et al.*, Physical Review Letters **125**, 155003 (2020).
[14] B. J. MacGowan, (submitted to HEDP).
[15] D. D. Ho, Bull. Am. Phys. Soc. 52(16), 273 (2007);
[16] A. J. MacKinnon *et al.*, Physics of Plasmas (1994-present) **21**, 056318 (2014).
[17] J. S. Ross *et al.*, Physical Review E **91**, 021101 (2015).
[18] L. F. Berzak Hopkins *et al.*, Physical Review Letters **114**, 175001 (2015).
[19] D. D. M. Ho, S. W. Haan, J. D. Salmonson, D. S. Clark, J. D. Lindl, J. L. Milovich, C. A. Thomas, L. F. B.

Hopkins, and N. B. Meezan, Journal of Physics: Conference Series **717**, 012023 (2016).
[20] N. B. Meezan *et al.*, Physics of Plasmas **22**, 062703 (2015).
[21] L. Divol *et al.*, Physics of Plasmas **24**, 056309 (2017).
[22] L. F. Berzak Hopkins *et al.*, Physics of Plasmas **22**, 056318 (2015).
[23] A. L. Kritcher *et al.*, Physics of Plasmas **25**, 056309 (2018).
[24] H. F. Robey, L. Berzak Hopkins, J. L. Milovich, and N. B. Meezan, Physics of Plasmas **25**, 012711 (2018).
[25] D. T. Casey *et al.*, Physics of Plasmas **25**, 056308 (2018).
[26] K. L. Baker *et al.*, Physical Review Letters **121**, 135001 (2018).
[27] A. L. Kritcher *et al.*, Physics of Plasmas **27**, 052710 (2020).
[28] D. S. Clark *et al.*, Physics of Plasmas **21**, 112705 (2014).
[29] C. Young et al., submitted to POP.
[30] R. C. Shah *et al.*, Physical Review Letters **118**, 135001 (2017).
[31] D. T. Michel *et al.*, Physical Review Letters **120**, 125001 (2018).
[32] H. Huang, R. B. Stephens, S. A. Eddinger, J. Gunther, A. Nikroo, K. C. Chen, and H. W. Xu, Fusion Science and Technology **49**, 650 (2006).
[33] H. Huang, B. J. Kozioziemski, R. B. Stephens, A. Nikroo, S. A. Eddinger, K. C. Chen, H. W. Xu, and K. A. Moreno, Fusion Science and Technology **51**, 519 (2007).
[34] B. J. Kozioziemski, J. A. Koch, A. Barty, H. E. M. Jr., W.-K. Lee, and K. Fezzaa, Journal of Applied Physics **97**, 063103 (2005).
[35] B. J. Kozioziemski, J. D. Sater, J. D. Moody, J. J. Sanchez, R. A. London, A. Barty, H. E. Martz, and D. S. Montgomery, Journal of Applied Physics **98**, 103105 (2005).
[36] T. Parham *et al.*, Fusion Science and Technology **69**, 407 (2016).
[37] A single projection view from a contact radiograph of this shell showed a mode-1 amplitude of 0.55 ± 0.2 %. Because the contact radiograph is from a single projection these values cannot be compared directly. However using a statistical argument of randomly aligned and projected mode-1 values onto a single view, the single view is most likely to be 79% of the total amplitude and so we can infer a range of values within a typical 1 sigma error of 0.7 +0.6/-0.2 % (including the diagnostic uncertainty). The agreement between the two approaches gives confidence in the fidelity of this challenging measurement.
[38] B. K. Spears *et al.*, Physics of Plasmas (1994-present) **21**, 042702 (2014).
[39] M. M. Marinak, G. D. Kerbel, N. A. Gentile, O. Jones, D. Munro, S. Pollaine, T. R. Dittrich, and S. W. Haan, Physics of Plasmas **8**, 2275 (2001).
[40] C. R. Weber *et al.*, Physics of Plasmas **27**, 032703 (2020).
[41] The slight offset at the center (hotspot velocity at zero m1 asymmetry) is due to the inclusion of other perturbations in the capsule (including a surrogate model for the fill-tube) and drive in this post-shot simulation and numerical error.
[42] O. A. Hurricane *et al.*, Physics of Plasmas **24**, 092706 (2017).
[43] S. P. Hatchett, *Ablation gas dynamics of low-Z materials illuminated by soft x-rays* 1991).
[44] C. B. Yeamans and D. L. Bleuel, Fusion Science and Technology **72**, 120 (2017).
[45] H. G. Rinderknecht, D. T. Casey, R. Hatarik, R. M. Bionta, B. J. MacGowan, P. Patel, O. L. Landen, E. P. Hartouni, and O. A. Hurricane, Physical Review Letters **124**, 145002 (2020).
[46] <x,y,z> in units of km/s through the determined sensitivity of drive to hotspot velocity.
[47] The hotspot velocity to seed relationship becomes non-linear around ~100 km/s as is evident in Fig. 3. While some nonlinear behavior may be present in the data set, only two absolute hotspot velocities >100 km/s and so we expect this to play a minor role, possibly contributing some noise to the hotspot to shell asymmetry sensitivity.
[48] The capsule mode 1 value does not include a 5% contribution in the denominator (mode 1) for DT fuel mass, or any mode 1 thickness variation in the DT fuel, which is typically <1% so usually insignificant.
[49] T. J. Murphy, Physics of Plasmas (1994-present) **21**, 072701 (2014).
[50] A. B. Zylstra *et al.*, Physics of Plasmas **27**, 092709 (2020).
[51] Hohenberger et al., accepted for publication in Physics of Plasmas
[52] Zylstra et al., submitted to Physical Review Letters.